Novel methods of intracavity beam shaping

R. John Koshel*
Breault Research Organization, Inc.

ABSTRACT

Methods of shaping laser beams within the laser resonator are studied. The simplest form of shaping is the spatial mode generation inherent in the laser cavity due to the geometry of the resonator in conjunction with gain to compensate for roundtrip losses, such as diffraction and output coupling. Typically the fundamental mode or multimode behavior is exhibited from such configurations. Passive mode shaping can be accomplished by introducing static amplitude or phase masks. An example of an amplitude mask is provided in order to generate a higher-order spatial mode. Active mode shaping can be accomplished by altering the optical pump distribution. This case is studied experimentally with a diode-end-pumped Nd:YVO_4 laser and compared to modeling of expected Hermite-Gaussian mode generation. Active mode shaping allows the preferred mode distribution to be altered in real time. Additional shaping can be done following the resonator to modify a Hermite-Gaussian mode into a psuedo-Laguerre-Gaussian mode. This work also shows that using the coherent propagation method of Gaussian beam decomposition is capable of modeling and describing intracavity beam shaping.

Keywords: laser beam shaping, transverse modes, solid-state lasers, laser resonator, coherent propagation, Hermite-Gaussian mode, Laguerre-Gaussian mode

1. INTRODUCTION

The typical method of laser beam shaping is done external to the cavity in order to obtain a laser beam with the desired spatial distribution and propagation characteristics. A more efficient method to shape a laser beam is to do the shaping within the resonator. This method will ensure that the gain is coupled preferentially into the prescribed spatial mode distribution, thus diffraction and other losses are minimized. The primary difficulty with modeling the shaping within the resonator is that the coherent aspects of the beam must be retained, unlike extracavity beam shaping which typically uses a geometric ray-based approach to model the dynamics of the system.[1] The coherent propagation requirement means that both the amplitude and phase must be retained with every roundtrip within the resonator. This process can be laborious, but fortunately there is a method based on geometrical ray tracing whereby both phase and amplitude are propagated along descriptor rays. This method is called Gaussian beam decomposition (GBD).[2-4] It is based on the propagation of a number of Gaussian beams (Gauslets) that are summed coherently to generate the field distribution, and thus irradiance distribution, at any location. The Gauslets have a number of descriptor rays: base, waist, and divergence; that govern how Gaussian beams propagate. GBD is available in the Advanced Systems Analysis Program (ASAP) commercial software from Breault Research Organization, Inc.[5]

There are a number of methods to do intracavity beam shaping. First and foremost is the spatial mode generation of the simple resonator. This configuration includes the two mirrors (high reflector and output coupler) and the laser gain medium (solid-state is studied herein). The shape of the two mirrors and their reflectivities in conjunction with the gain profile play the primary role in the generation of the spatial mode distribution. Typically, solid-state lasers have a cylindrical geometry, including both the mirrors and gain medium. One would expect the output of the laser to have a radial spatial profile, such as a Laguerre-Gaussian (LG) modes, but due to material and geometrical asymmetries (e.g., index of refraction and tilt respectively) in the laser, the spatial mode distribution tends to be Cartesian in nature. This result means that solid-state lasers prefer to lase in the Hermite-Gaussian (HG) basis set.[6] Unfortunately, simple laser resonators do not exhibit single mode output, but, rather, multimode behavior. Multimode output is the combination of several individual modes of the resonator. These spatial modes have some degree of coherence between them; however, one typically sums them together incoherently. The reasoning is once again due to the asymmetries of the laser resonator, so that each transverse mode tends to oscillate at a different optical frequency. One method to alleviate the dispersion of the laser resonator is to use a symmetric confocal configuration. In theory, the symmetric confocal resonator should oscillate at the same wavelength for

* jkoshel@breault.com; phone 1 520 721-0500; fax 1 520 721-9630; http://www.breault.com' Breault Research Organization, Inc., Suite 350, 6400 East Grant Road, Tucson, AZ 85715

each spatial mode. Therefore, one can (in theory) coherently add modes together in such a configuration, and due to the nature of a complete basis set in both the HG and LG forms, one can add these beams together to generate any desired beam shape. HG and LG beams exhibit several other interesting properties, such as they maintain their shape with propagation, but they remain beyond the scope of this article.[7]

Numerous analytic and numerical methods have been employed to determine the transverse mode behavior of simple laser resonators. They include, but are not limited to: Schawlow and Townes,[8] Fox and Li,[9] and Boyd and Gordon.[10] For example, in the Fox and Li method of Ref. 9 a plane wave is started between two planar mirrors. Several roundtrips of this field distribution are numerically modeled such that the diffraction affects of the end mirrors can be taken into account. Depending on the layout of the resonator, in particular the mirror sizes and cavity length, the original planar wavefront will converge to a particular spatial mode distribution. Other methods, such as Boyd and Gordon of Ref. 10 for confocal resonators, looked at different special cases to determine the spatial mode distribution coming from a laser resonator. Analogously, commercial software such as ASAP can be used to investigate models for any arbitrary geometry for the resonator. Therefore, with this software package, one is not restricted to special cases, but one can investigate how the basic shape of the resonator affects mode generation.

The next step in intracavity beam shaping is to place amplitude and phase masks within the resonator to shape the output into a desired pattern. The primary example is the inclusion of a circular aperture of a prescribed diameter to inhibit higher-order transverse modes due to diffraction losses while preferentially propagating the fundamental mode (TEM_{00}). Other examples of amplitude masks include placing wires within the resonator to select a desired HG mode.[11] Phase masks can also be introduced typically as the reflective high reflector or less often as a transmissive intracavity element.[12] In both cases the phase mask is a diffractive element that modifies the preferred phase structure of the resonator.

All of the previously described methods are hereafter called passive methods of intracavity laser beam shaping. They are called passive because a static intracavity element, phase or amplitude, is added to shape the oscillating beam. There is dynamic ability to shape the beam with intracavity elements. Using active intracavity elements such as spatial light modulators and electro-optic cells allow the laser designer in theory to modify the laser beam to a prescribed shape. Another method to accomplish this feat is by changing the absorption distribution of pump light within the gain medium. With this method it has been shown that by locating the gain to a preferred region that overlaps with a prescribed spatial mode, that mode is preferentially selected.[13] The technique employs an end-pumped, solid-state gain medium with a resonator built around it. Altering the transverse location of a pump source such as a laser diode alters the pump region in real time.

Finally, one can shift HG-mode output to pseudo-LG-mode output with the use of an cylindrical optical processor that introduces twist into the laser output. This technique takes a subjectively unappealing asymmetric mode distribution and modifies it into an elliptical irradiance distribution. These altered modes have uses in machining and marking, lithography, and trapping of particles. Additionally, it has been speculated that the coherent combination of three modes from a distinct basis set can be added to effectively make a delta-function beam.[14] This beam would propagate as this "delta-function" due to the propagation properties of Gaussian beams, thus it has immediate uses in direct-write lithography.

In the next section the method of coherent propagation, GBD, is discussed in more detail. Following this section is a treatment of passive intracavity beam-shaping methods. Section 4 discusses active beam shaping, while Section 5 gives an introduction of an extracavity method to introduce a degree of symmetry into the output. Finally, this paper ends with conclusions.

2. GAUSSIAN BEAM DECOMPOSITION

Gaussian beam decomposition is a method to propagate both amplitude and phase with a ray-tracing approach. It makes use of Gauslets to propagate a portion of a full field distribution. The Gauslets are summed at desired locations, and the irradiance distribution is found including interference effects. As mentioned previously, ASAP uses this technique to propagate coherent fields.

Since Gaussian beams are a solution of the scalar wave equation and they maintain their shape as they propagate through optical systems, they provide a logical method for decomposition of a real field. The Gauslets are selected to provide an overlap in the original distribution plane such that the coherent summation of the Gauslets gives the desired irradiance distribution. There are a number of rays that describe the propagation of the individual Gauslets: base, waist, and divergence.

The base ray is the defining ray of the Gauslet since it propagates normal to the Gauslets peak field point. The waist and divergence rays are called parabasal rays. For any Gauslets there are up to eight parabasal rays, four waist rays and four divergence rays. The waist rays are divided into the two orthogonal transverse directions of the Gauslet distribution. These four rays are positioned at the waist locations in irradiance space (i.e., e^{-2}) for the Gauslet. Thus, the two rays for a given transverse direction can be used to introduce mirror asymmetry, while differences in the waist widths for the orthogonal directions introduce astigmatism. It is likewise for the divergence rays, but they asymptotically approach the extent of the diverging wavefront of the Gauslet. Figure 1 shows how these rays are positioned and directed for an individual Gauslet. Most applications only require four rays.

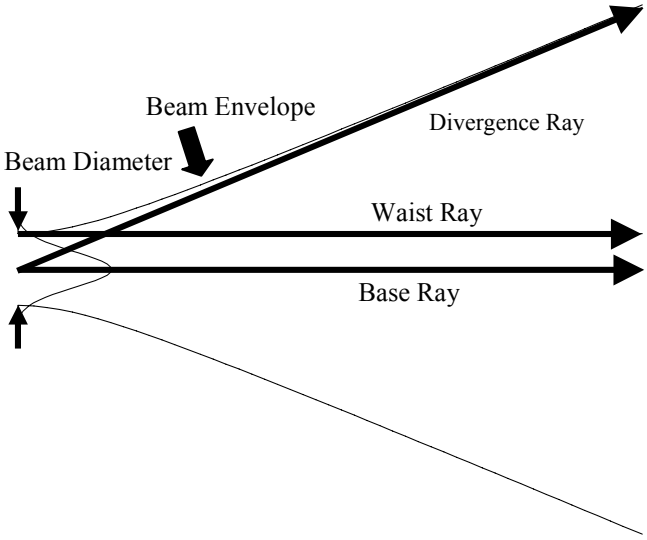

Figure 1. The rays describing a Gauslet for GBD.

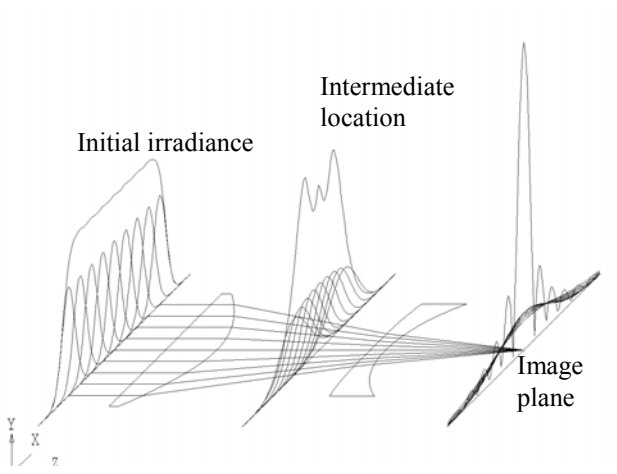

Figure 2. Example of propagation of multiple Gauslets through two lenses from input to image plane.

As the Gauslets propagate their directions and sizes change dependent on the optical properties of the various media that they are incident upon, as shown in Fig. 2. In this case the initial pseudo-flat-top irradiance distribution is the combination of many individual Gauslets. Upon transfer through the positive lens, the wavefront is converging toward some point in space. The irradiance distribution is shown for an arbitrary position after this lens. The Gauslets then propagate through a second lens that brings them to focus at the last plane. Note the characteristic Airy distribution for the focal spot that arises due to the coherence of the input beam. Often the field distribution has to be decomposed to take into account the widening of each Gauslet. As is evidenced in Fig. 2, the Gauslets are getting wider as they propagate. In order to compensate for this problem, resampling of the beam space must be done to effectively "see" small-scale structure. Therefore, GBD requires that the designer understand how the optical system evolves during propagation. In the cases to be studied hereafter, the field distribution must be decomposed at each instance of an object being struck – the two end mirrors, gain medium, and intracavity amplitude or phase masks. Additionally, decomposition in direction space can be done when a structure is suitably small such that one is more interested in the spatial frequencies that are transmitted through the object. Pinhole apertures in spatial filters are an example of where directional decomposition is required. Note that directional decomposition was not required for the study discussed herein.

In the next section GBD is employed to study standard, passive intracavity beam-shaping configurations. The Fox-Li case of plane-parallel mirrors is the first investigation, followed by the investigation of a near planar-mirror case. Finally, an investigation of inserting a wire to select a higher-order spatial mode is done.

3. PASSIVE INTRACAVITY LASER BEAM SHAPING

In order to understand how GBD works with passive intracavity beam shaping, distinct examples are studied. The cases can employ any particular parameters, but three arbitrary cases are studied in this section:

1. A Fox-Li configuration employing plane-parallel mirrors. The mirrors are 10 mm in diameter with a 1-m distance between them. The wavelength of light is 1 μm. The initial field is flat over the extent of the mirrors. This configuration has a Fresnel number of 23.85. Arbitrary gain of 0.6% is provided on each roundtrip.

2. A configuration employing one flat mirror and the other mirror with a 10-m radius of curvature. The flat mirror is the limiting factor and is elliptical in shape: 7.071 mm by 5 mm. The length of the resonator is 1.25 m. The wavelength of light is 1.06 μm. The initial field is flat over the extent of the planar mirror. The configuration has a Fresnel number of 10. Arbitrary gain of 1.875% is provided one each roundtrip.
3. A plano-concave configuration with the flat mirror being the high reflector and the other mirror having a radius curvature of 250 mm. The separation between the two mirrors is 212 mm. The diameter of the limiting flat mirror is 1.408 mm. The wavelength of light is 1.06 μm. The fundamental mode has a radius of 176 μm at the flat mirror. An absorbing wire is placed at the concave mirror to select the $HG_{2,0}$ mode. The initial field is the fundamental mode of the resonator.

The first case investigates the ability to model the Fox-Li approach. The second case shows how ASAP is not limited to special cases since it introduces radial asymmetry in one mirror for a plano-concave resonator. The last case shows intracavity elements can be used to shape the oscillating beam.

The input irradiance distribution for cases 1 and 2 is shown in Fig. 3. Note that the diameter of the flat-top input is over 10 mm, thus it will cover the extent of the planar mirrors in both cases. The waist for this decomposition is set to be at the planar mirror. No additional parameters for each resonator are imparted to the input field. Figure 4 shows the resulting (a) irradiance and (b) wavefront for the first case (plane-parallel resonator), while Fig. 5 shows the analogous plots for the second case (plano-concave resonator with elliptical asymmetry). Both are shown after 250 roundtrips. The wavefront for case 2 (Fig. 5b) is at the planar mirror.

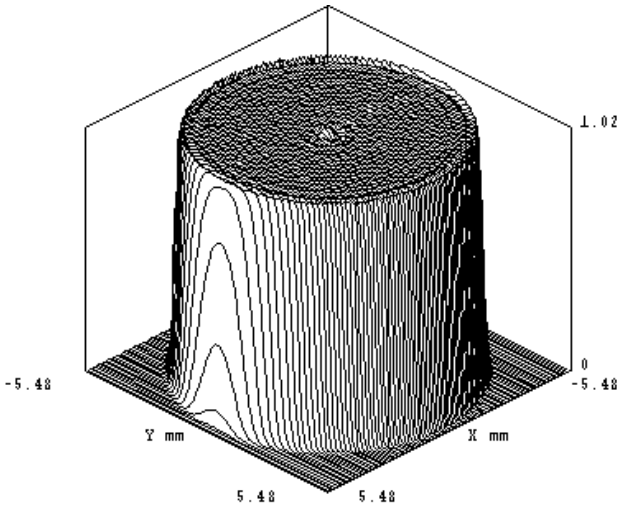

Figure 3. Input irradiance distribution for cases 1 and 2.

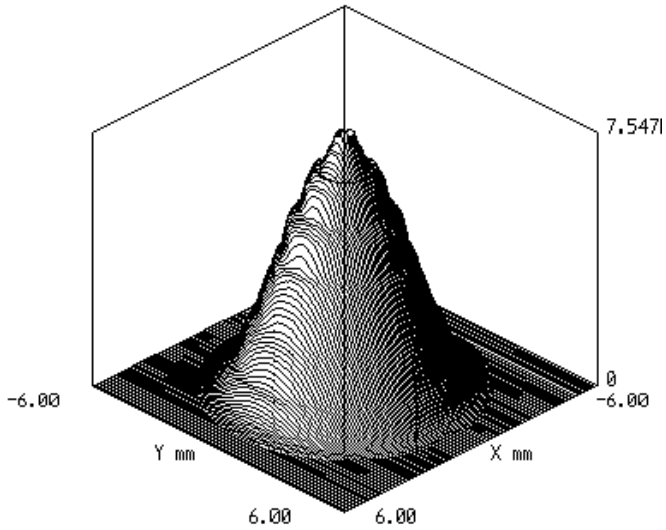

(a) Irradiance distribution

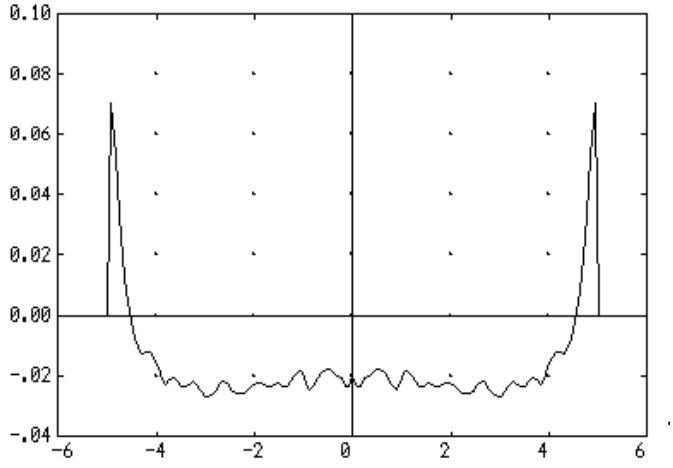

(b) Wavefront profile

Figure 4. The (a) irradiance distribution and (b) wavefront profile at one of planar mirrors for case 1. These results are shown after 250 roundtrips within the resonator and 0.6% gain per roundtrip. The horizontal axes are posiitons in mm, while the vertical axes in (a) is flux per square mm and in (b) it is wavefront in units of lambda.

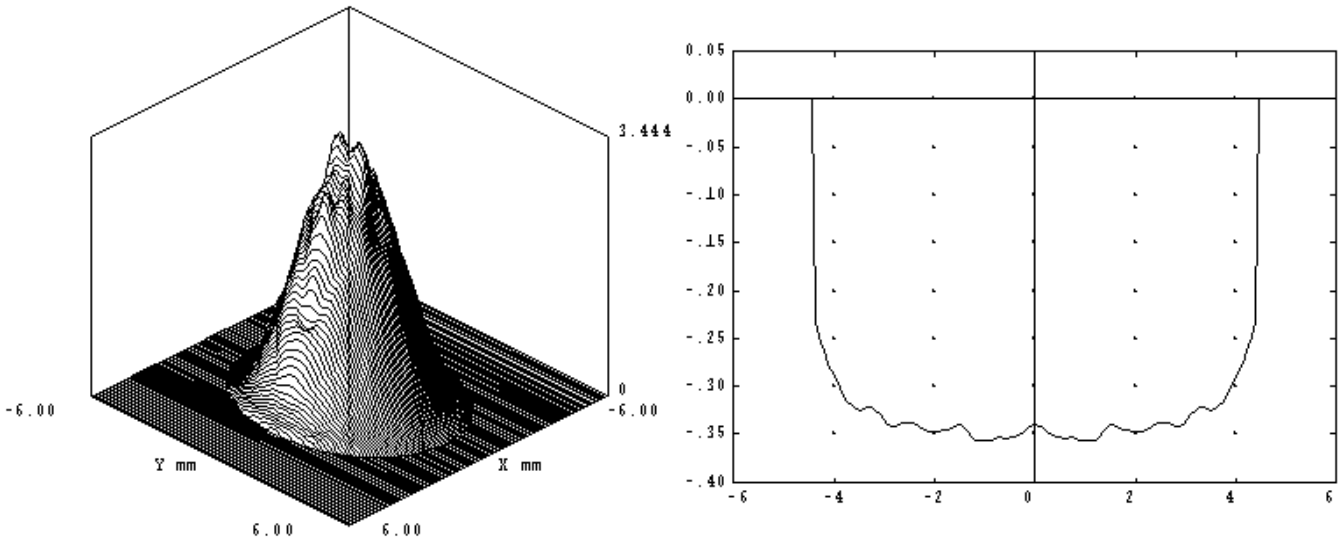

(a) Irradiance distribution (b) Wavefront profile

Figure 5. The (a) irradiance distribution and (b) wavefront profile at the planar mirror for case 2. These results are shown after 250 roundtrips within the resonator and 1.875% gain per roundtrip. The horizontal axes are positions in mm, while the vertical axes in (a) is flux per square mm and in (b) it is wavefront in units of lambda.

In both Figs. 4 and 5 there is still rippling on the three-dimensional irradiance distribution. More roundtrips would alleviate some of this rippling; however, the diffraction inherent in each resonator is giving rise to a portion of it. Note that Fig. 5a shows the asymmetry due to the shape of the planar mirror. In both Figs. 4 and 5 the wavefront exhibits some curvature toward the edges of the mirror. This result is to be expected in light of the results of Fox and Li.[9,15]

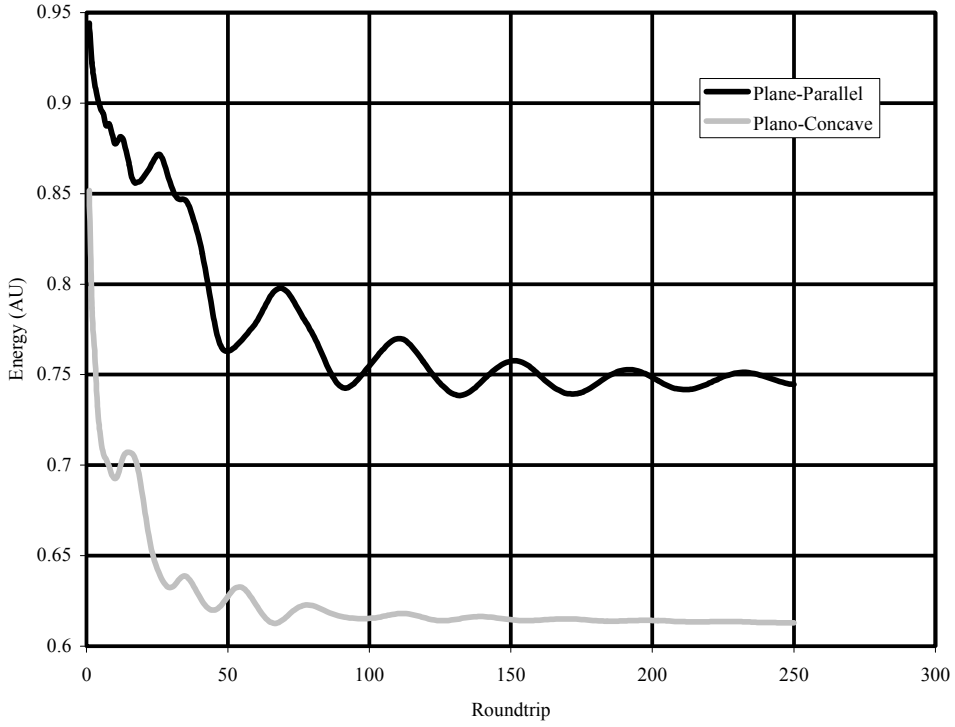

Figure 6. Convergence as function of roundtrips for case 1 (plane-parallel/black curve) and case 2 (plano-concave/gray curve).

An issue of importance is the speed of convergence for these cases, since GBD can be time consuming as one increases the sampling of the coherent beam. For the first two cases the data for the energy contained within the spatial distribution was saved for each roundtrip. The results are plotted in Fig. 6. The black line is for case 1 while the gray line is for case 2. Note that the energy values are arbitrary for both cases, and were knowingly offset from one another in order to allow discrimination between the two curves. The plane-parallel case is slow to converge while the plano-concave case converges much more rapidly. In fact the plano-concave case has converged after about 150 roundtrips while the plane-parallel case has still not converged after 250 roundtrips. It is speculated that plane-parallel

case would require around 350 roundtrips to converge. The gain per roundtrip compensates for the diffraction upon convergence. These curves are similar to the results that Fox and Li found; thus, ASAP is quite capable of modeling the intracavity dynamics of a laser. Case 1 is slower to converge than case 2 due to the higher Fresnel number. This higher the Fresnel number the less diffraction loss per pass, so more roundtrips are required to converge to the eigenstate of the resonator.

Case 3 was the next investigation. As discussed previously, a near hemispherical resonator is designed such that the waist is located near the planar mirror. This laser cavity configuration is used in numerous solid-state lasers in order to provide stability while not exceeding the damage threshold of the gain medium and the coating on the planar mirror. The input is the fundamental mode of the resonator (w_0 = 176 μm at the planar mirror) as shown in Fig. 7. A wire is placed at the minimum between the central and one of the exteriors lobe of the $HG_{2,0}$ mode. After multiple roundtrips, this absorbing wire should only allow the $HG_{2,0}$ mode for oscillation. Other modes would not resonate due to large diffraction losses introduced by the wire. Additionally, the planar mirror diameter was selected to be four times the fundamental mode radius at this mirror. This choice allows the fundamental mode in the direction parallel to the wire while inhibiting higher-order mode generation. A general rule of thumb is to have the aperture at least three times the size of the propagating beam, but the larger the factor the less diffraction ripple will be evident on the beam profile. Too large of an aperture will allow the higher-order modes to start oscillating, which is required in this case. Figure 8 shows the resulting (a) irradiance distribution and (b) wavefront profile after 150 roundtrips. Note that the irradiance distribution shows the characteristic three lobes of the $HG_{2,0}$ mode. The wavefront profile is nearly flat, as expected, over the extent of the beam. The conclusion is that ASAP is able to model intracavity passive, amplitude masks, thus allowing the designer to optimize the performance of the laser and any desire beam shaping before fabrication of the system.

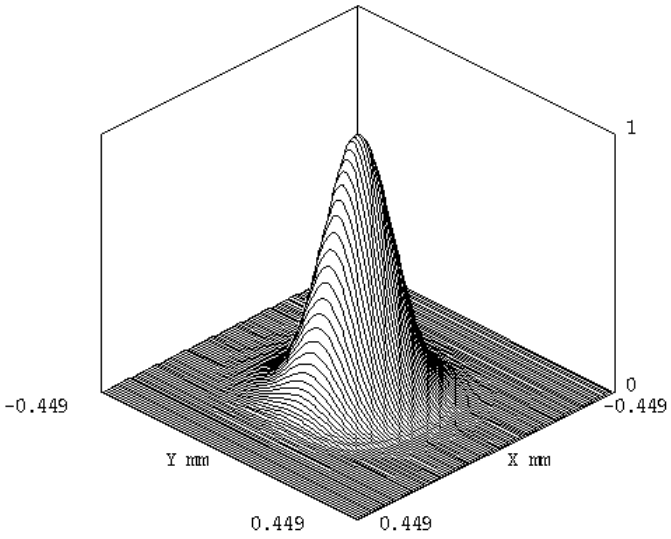

Figure 7. Input irradiance distribution for case 3. It is the fundamental mode distribution for this resonator configuration.

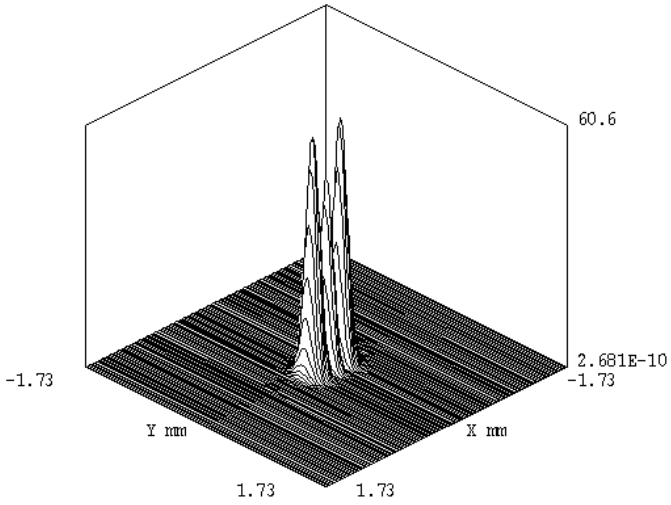

(a) Irradiance distribution

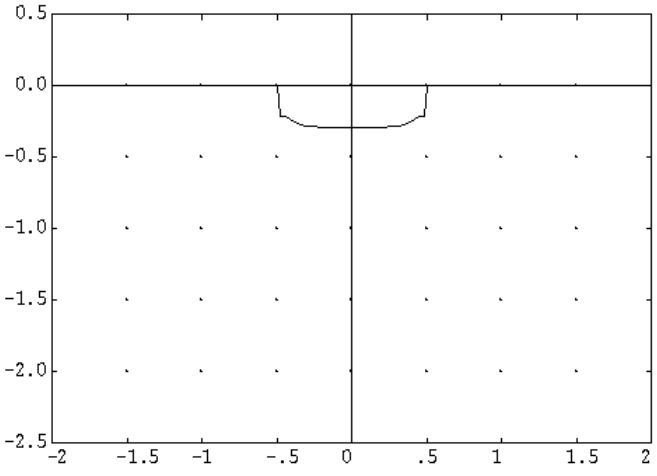

(b) Wavefront profile

Figure 8. The (a) irradiance distribution and (b) wavefront profile at the planar mirror for case 3. These results are shown after 150 roundtrips within the resonator. The horizontal axes are positions in mm, while the vertical axes in (a) is flux per square mm and in (b) it is wavefront in units of lambda.

4. ACTIVE INTRACAVITY LASER BEAM SHAPING

By changing the absorption distribution in real time, one is able to select the preferred HG mode for output. By localizing the gain profile an effective aperture is created, similar to case 3 in the previous section. It has been shown theoretically that one can determine the input power required to obtain a certain laser output for prescribed absorption and mode distributions.[16] The functional relationship is

$$\frac{1}{P_{in}} = \frac{4\eta}{P_{sat} L} \int_0^{2\pi} \int_0^{\infty} \frac{g(r,\theta) f(r,\theta) / A_p}{1 + 4 P_{out}\ f(r,\theta) / P_{sat} T_{oc}} r dr d\theta \,, \tag{1}$$

where P_{in} is the input power, P_{out} is the output power, P_{sat} is the saturation power of the gain medium, L is the total roundtrip loss, T_{oc} is the transmission of the output coupler, $g(r,\theta)$ is mode distribution in radial coordinates, $f(r,\theta)$ is the mode distribution, A_p is the pump area, and η is the transfer efficiency of pump light to the upper state. This equation is valid in the low-gain approximation, which means T_{oc} is limited to appoximately less than 30%. The threshold and slope efficiciency near threshold are given by

$$P_{th} = \frac{P_{sat} L}{4\eta} \left[\int_0^{2\pi} \int_0^{\infty} g(r,\theta) f(r,\theta) / A_p \, r dr d\theta \right]^{-1} \tag{2}$$

and

$$\eta_{s,th} = T_{oc} L \left(\frac{P_{sat}}{4\eta P_{th}} \right)^2 \left[\int_0^{2\pi} \int_0^{\infty} g(r,\theta) f^2(r,\theta) / A_p \, r dr d\theta \right]^{-1} , \tag{3}$$

respectively. The threshold-input power is simply the reciprocal of the overlap integral of the gain and mode distributions. The slope efficiency is the reciprocal of the gain distribution and the square of the mode distribution. A laser designer typically desires to have a low threshold and a high slope efficiency; however, Eqs. (2) and (3) do not allow this desire. One can have a low threshold, but slope efficiency will therefore decrease. The high slope efficiency case means that the threshold will increase. Thus the laser designer must design the laser for the required output power to get the highest overall efficiency and not worry about the individual parameters of threshold and slope efficiency.

The above equations indicate that increasing the overlap of the pump distribution with the higher-order mode distribution results in these modes being generated. Figure 9 shows the mode distributions for three HG modes: (0,0), (10,0), and (50,0). Also indicated is the pump width of an end-pumped, solid-state chip laser as shown in Fig. 10. By locating the pump light in the outer lobe of a given mode, that mode will

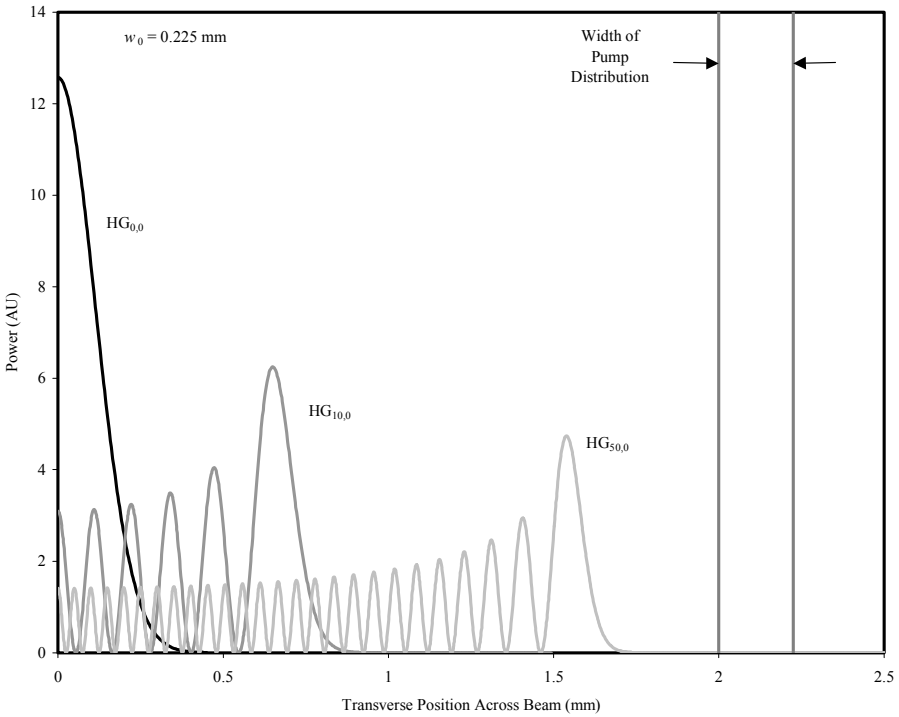

Figure 9. Mode distributions for the $HG_{0,0}$, $HG_{10,0}$, and $HG_{50,0}$ modes. The width of the pump distribution resulting from the configuration in Fig. 10 is shown.

oscillate before others. In fact, the overlap is so much higher than for other modes, that a single mode is typically generated until the pump power is too high. One can change the preferred mode in real time by moving the laser diode laterally across the solid-state gain medium. In this setup a dichroic coating is placed on the back of the gain medium. It passes the pump radiation (808 nm) and reflects the laser radiation (1064 nm).

A series of examples were modeled in ASAP. The pump distribution is determined via ray tracing such that the pump-mode overlap can be calculated as the laser diode is moved off axis. The experimental results and corresponding software models for three cases are shown in Fig. 11. These examples use the laser cavity properties of case 3 from Section 3 for an Nd:YVO_4 laser. Up to the $HG_{201,0}$ mode has been generated with this laser, with diffraction being the ultimate limiting factor in higher-order mode generation. At this juncture more modeling is required to better understand the curvature of the lobes for higher-order modes and to understand the alignment tolerances.

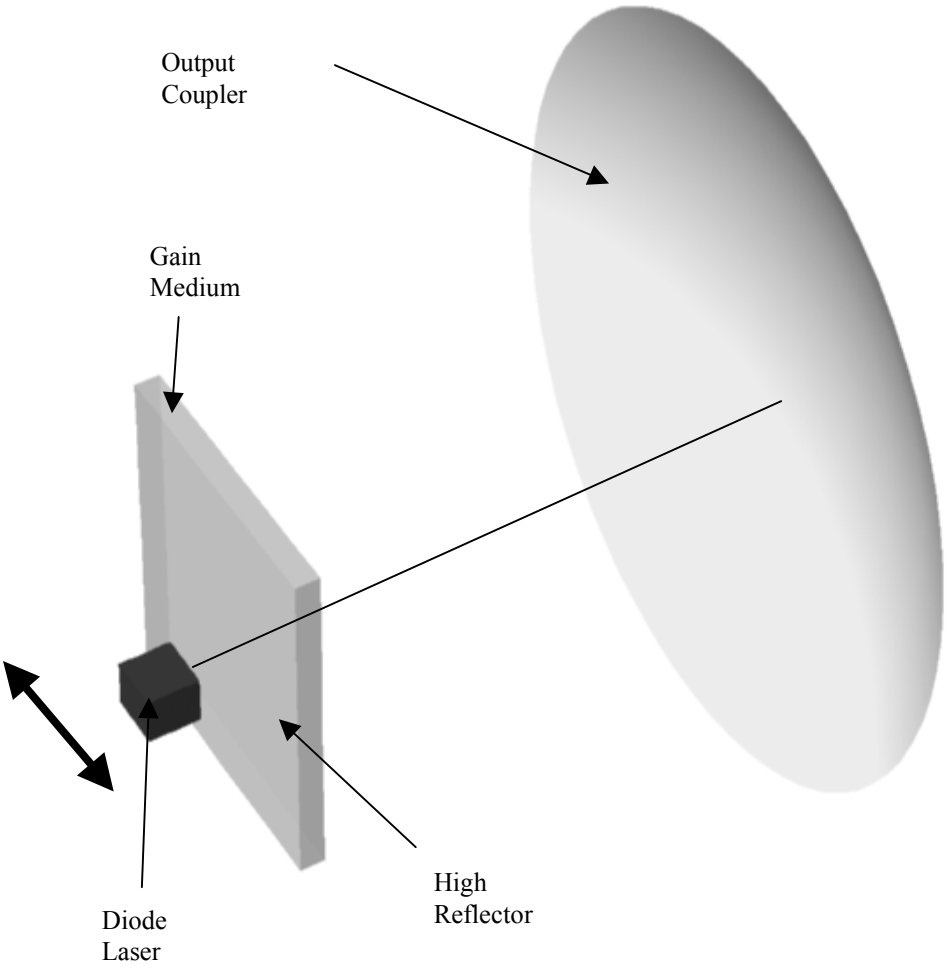

Figure 10. Configuration for the active intracavity laser-beam shaper, which uses the pump distribution to select the preferred HG spatial mode in real time.

The output power as a function of input power for HG modes up to (20,0) is shown in Fig. 12. Note that the (1,0) mode displays the best performance, most likely due to better alignment and thus better overlap of the pump distribution with the mode profile. Also, the power output decreases as the input power is increased above certain values for each mode. The most likely reason is thermal issues, including birefringence and lensing. More study is required to better understand the thermal issues with higher-order mode generation from this type of laser. Additionally, the mode content as a function of input power needs to be investigated – including mode competition for the available gain.

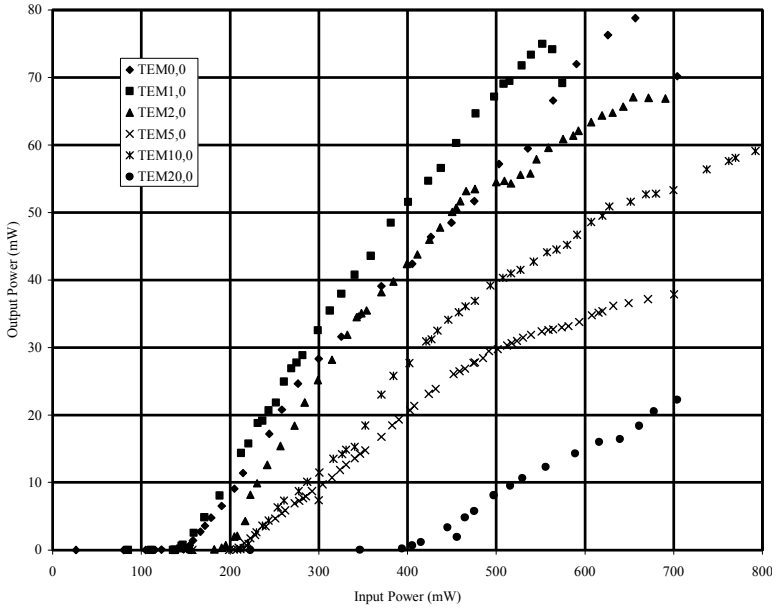

Figure 12. Output power as a function of input power for several higher-order modes.

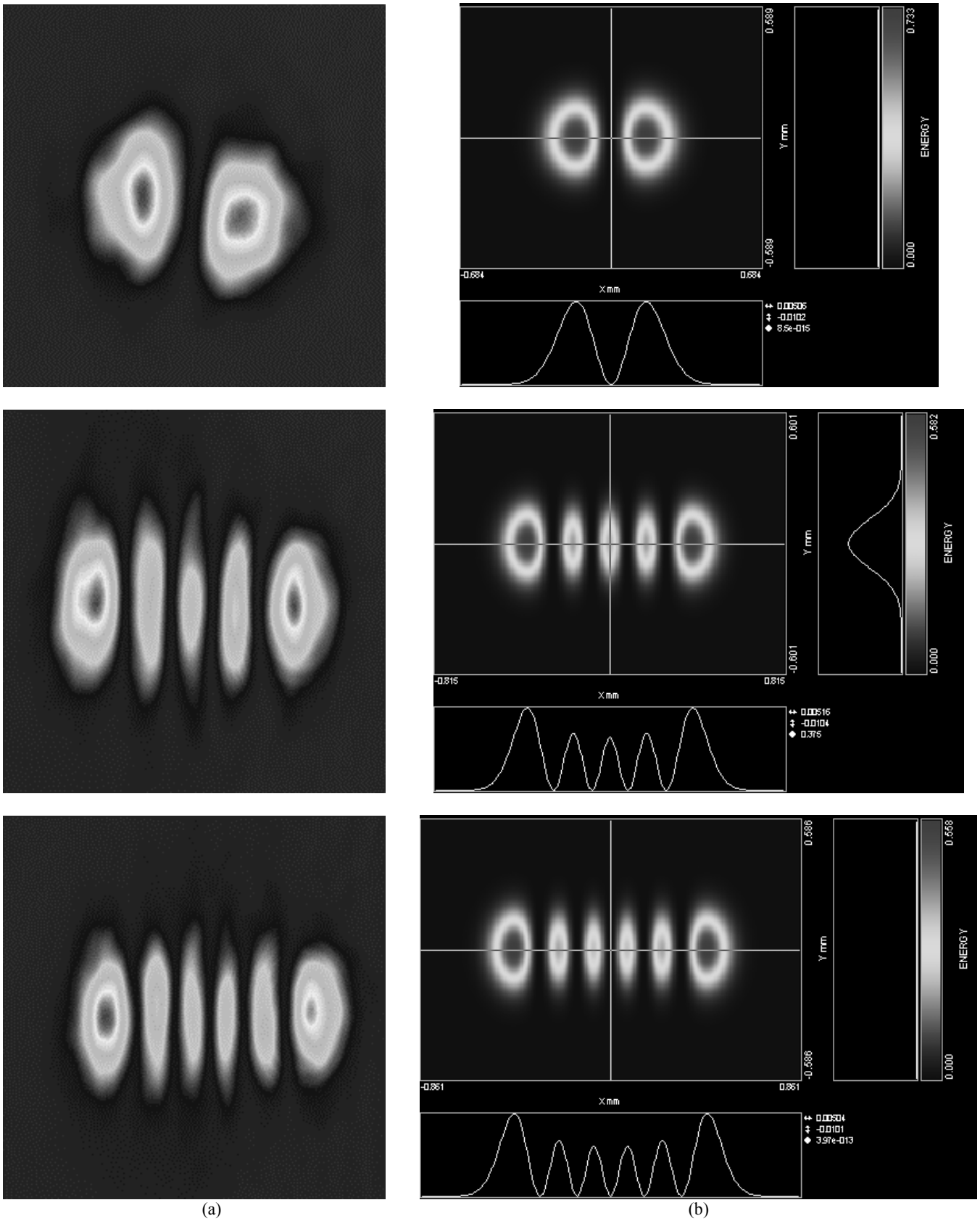

(a) (b)

Figure 11. Higher-order HG output for the (1,0), (4,0), and (5,0) modes: (a) experimental and (b) software modeling.

5. EXTRACAVITY LASER BEAM SHAPING

The HG modes generated in the previous section have limited real-world utility. A possible application is a spot array generator for an optical communication application. It would be more useful to generate a mode pattern with a high degree of radial symmetry. One can convert the HG modes from the previous section into LG modes by introducing a "twist" into the beam. The optical processor capable of doing this feat is shown in Fig. 13. Note the use of three cylindrical lenses with the respective spacing and focal lengths to accomplish this task. In this figure the input and output irradiance distributions are shown for one example. The input is the $HG_{4,0}$ mode with the output being a pseudo Laguerre-Gaussian mode. A twist has been introduced to the normal propagation of the laser output, so this mode evolves as it propagates. Multiple other configurations, input beams, and mode processor configurations are open to investigation. Additionally, the coherent combination of modes can be considered with such an optical processor, which would open new avenues for laser beam shaping.

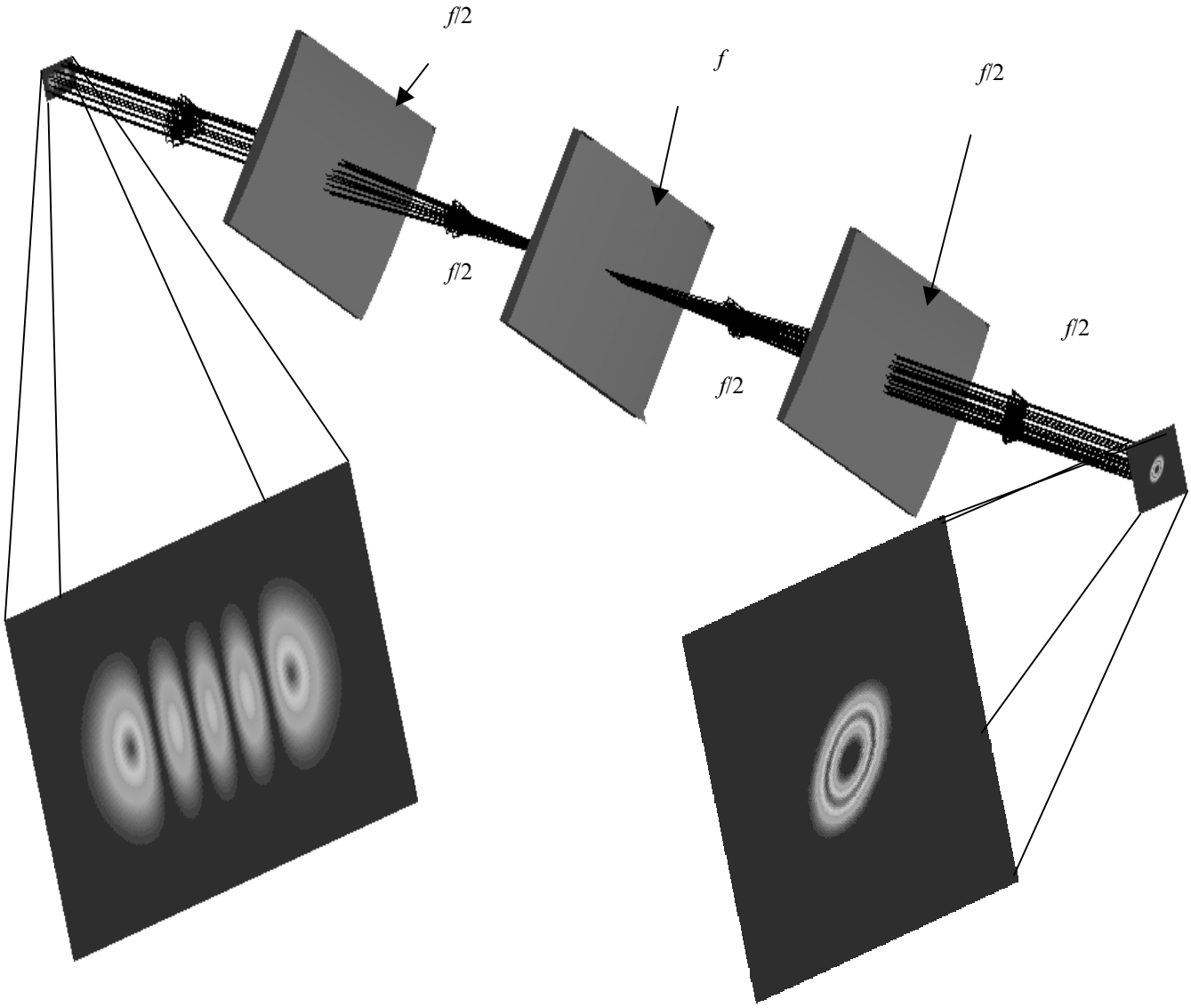

Figure 13. The optical processor comprised of three cylindrical lenses to transform HG modes into pseudo-LG modes. The coherent combination of modes with such a processor is open for investigation.

6. CONCLUSIONS

This paper has shown that intracavity laser beam shaping both through passive and active means is a viable means to shape laser output. Intracavity laser beam shaping has the ability to increase the efficiency over extracavity beam shaping. Second, commercial software such as ASAP can be used to model complex systems such as laser resonators. Third, active intracavity beams shaping allows the output distribution to be analyzed in real time, so that the utility of optimization of the configuration can be ascertained before fabrication. Finally, extracavity beam shaping can be considered to transform one basis set of modes to another or to combine coherently several modes within the laser resonator. The field of intracavity beam shaping has barely been touched to this date, but with robust software codes such as ASAP available now it has the potential to develop into a new field.

ACKNOWLEDGEMENTS

The experimental data was a result of working in the laboratory of Dr. Richard Jones at NIST/Boulder.

REFERENCES

1. F. M. Dickey and Scott C. Holswade, Eds., *Laser Beam Shaping: Theory and Techniques*, Marcel Dekker, Inc. New York, 2000. In particular D. L. Shealy, "Geometrical Methods," Chapter 4 of this test.
2. J. A. Arnaud, "Nonorthogonal optical waveguides and resonators," *Bell System Tech. Jnl.*, Nov., p. 2311, 1970.
3. A. Greynolds, "Propagation of general astigmatic Gaussian beams along skew ray paths," *Diffractive Phenomena in Optical Engineering Applications*, Proc. SPIE Vol. **560**, pp. 33-50, 1985.
4. A. Geynolds, "Vector-formulation of ray-equivalent method for general Gaussian beam propagation," *Current Developments in Optical Engineering and Diffractive Phenomena*, Proc. SPIE Vol. **679**, pp. 129-133, 1986.
5. Advanced Systems Analysis Program, Breault Research Organization, Inc., Suite 350, 6400 East Grant Road, Tucson, AZ, 85715.
6. A. E. Siegman, *Lasers*, University Science Books, Mill Valley, CA, p. 648, 1986.
7. For further disscussion of this phenomenon and others, see Ref. 6, in particular Chapter 16 and 17.
8. A. L. Schawlow and C. H. Townes, *Phys. Rev.* **112**, p. 1940, 1958.
9. A. G. Fox and T. Li, *Bell System Tech. Jnl* **40**., p. 453, 1961.
10. G. D. Boyd and J. P. Gordon, *Bell System Tech. Jnl.* **40**., p. 489, 1961.
11. Numerous examples exist, see for example and the references contained therein: W. Koechner, *Solid-State Laser Engineering*, 4th Ed., Springer, Berlin, Germany, Chapter 5, pp. 189-280, 1996.
12. See the work of J. R. Leger; for example J. R. Leger, D. Chen, and Z. Wang, "Diffractive optical element for mode shaping of a Nd:YAG laser," *Opt. Lett.* **19**, pp.108-110, 1994.
13. H. Laabs and B. Ozygus. "Excitation of Hermite Gaussian modes in end-pumped solid-state laser via off-axis pumping," *Opt. and Laser Tech.* **28**, pp. 213-214, 1996.
14. R. Frieden, Optical Sciences Center, University of Arizona, private communication (1997).
15. W. Koechner, *Solid-State Laser Engineering*, 4th Ed., Springer, Berlin, Germany, p. 199, 1996.
16. R. J. Koshel and I. A. Walmsley, "Optimal design of optically side-pumped lasers," *IEEE Jnl of Quant. Elect.* **33**, pp. 94-102, 1997